Icarus 225 (2013) 850–855

Contents lists available at SciVerse ScienceDirect

Icarus

journal homepage: www.elsevier.com/locate/icarus

Note

Pacing early Mars river activity: Embedded craters in the Aeolis Dorsa region imply river activity spanned $\gtrsim$(1–20) Myr

Edwin S. Kite [a,*], Antoine Lucas [a], Caleb I. Fassett [b]

[a] Caltech, Division of Geological and Planetary Sciences, Pasadena, CA 91125, United States
[b] Mount Holyoke College, Department of Astronomy, South Hadley, MA 01075, United States

ARTICLE INFO

Article history:
Received 27 July 2012
Revised 27 March 2013
Accepted 28 March 2013
Available online 10 April 2013

Keywords:
Mars
Mars, Surface
Geological processes
Mars, Climate

ABSTRACT

We find net sedimentation rate $\lesssim$(13–200) μm/yr in the Aeolis Dorsa region, Mars, using the frequency of crater–river interactions. This sets a lower bound of 1–20 Myr on the total interval spanned by fluvial activity, which we correlate to the Noachian–Hesperian transition. The main uncertainty is the impact flux at the time of deposition. This result rules out basin-filling by a single catastrophic episode, such as a single impact-induced water–vapor greenhouse.

1. Introduction

On Mars, many craters are embedded within sedimentary sequences, leading to the recognition that the planet's geological history is recorded in "cratered volumes," rather than just cratered surfaces (Edgett and Malin, 2002). For a given impact flux, the density of craters interbedded within a geologic unit is inversely proportional to the deposition rate of that geologic unit (Smith et al., 2008). To use embedded-crater statistics to constrain deposition rate, it is necessary to distinguish interbedded craters from craters formed during and after exhumation. However, on Mars, erosion can exhume intact impact craters complete with ejecta blankets from beneath hundreds of meters of overlying sediment (e.g., Edgett, 2005). Variations in burial, exhumation, erosion, and (for icy targets) the presence or absence of viscous relaxation produce varying crater-preservation styles. Therefore it is difficult to determine which craters are syndepositional.

Regionally-integrated highland valley networks formed during a period of enhanced precipitation-fed runoff around the Noachian–Hesperian boundary ~3.6–3.7 Gyr ago (Irwin et al., 2005). This activity ceased planetwide at roughly the same time, perhaps even synchronously (Fassett and Head, 2011), although limited and/or localized fluvial activity continued afterward (e.g., Grant and Wilson, 2011; Mangold et al., 2012). Lake-basin hydrology disfavors valley-network formation by a single deluge (Barnhart et al., 2009; Matsubara et al., 2011). Improved constraints on the pace and persistence of fluvial activity during the Noachian–Hesperian transition are required to understand early Mars climate and habitability. It remains unclear whether the fluvial geomorphology of the Noachian–Hesperian transition is a palimpsest of transient events triggered by volcanic eruptions or impacts (Segura et al., 2008; Toon et al., 2010; Kite et al., 2011; Wordsworth et al., 2013), or alternatively records a sustained ($\gg$1 Kyr) wet interval(s) caused by unusual orbital conditions (Kite et al., 2013a), an early greenhouse (Sagan and Mullen, 1972), or an impact-triggered excursion to a warm stable state (Segura et al., 2012).

Here we use interactions between craters and fluvial deposits to determine sedimentation rate within a candidate Late Noachian/Early Hesperian sedimentary basin containing numerous fluvial deposits. A river flowing over a heavily cratered sedimentary landscape will be frequently diverted by crater rims and/or deposit sediment in pools corresponding to the crater interiors (Fig. 1). These craters, and craters partly overlain by river deposits, are readily identified as being syndepositional.

2. River–crater interactions

We search for river–crater interactions within exceptionally numerous and exceptionally well-preserved fluvial channel deposits exhumed by erosion in the Aeolis Dorsa region, formerly termed Aeolis–Zephyria Planum (Burr et al., 2009, 2010; note that we use Aeolis Dorsa to refer to the formally defined region, not just the ridges within that region). The area of our search (~6S, 152E; Fig. 2) is ~500 m below a surface with an Early Hesperian,

* Corresponding author.
E-mail address: ekite@caltech.edu (E.S. Kite).

0019-1035/$ - see front matter © 2013 Elsevier Inc. All rights reserved.
http://dx.doi.org/10.1016/j.icarus.2013.03.029

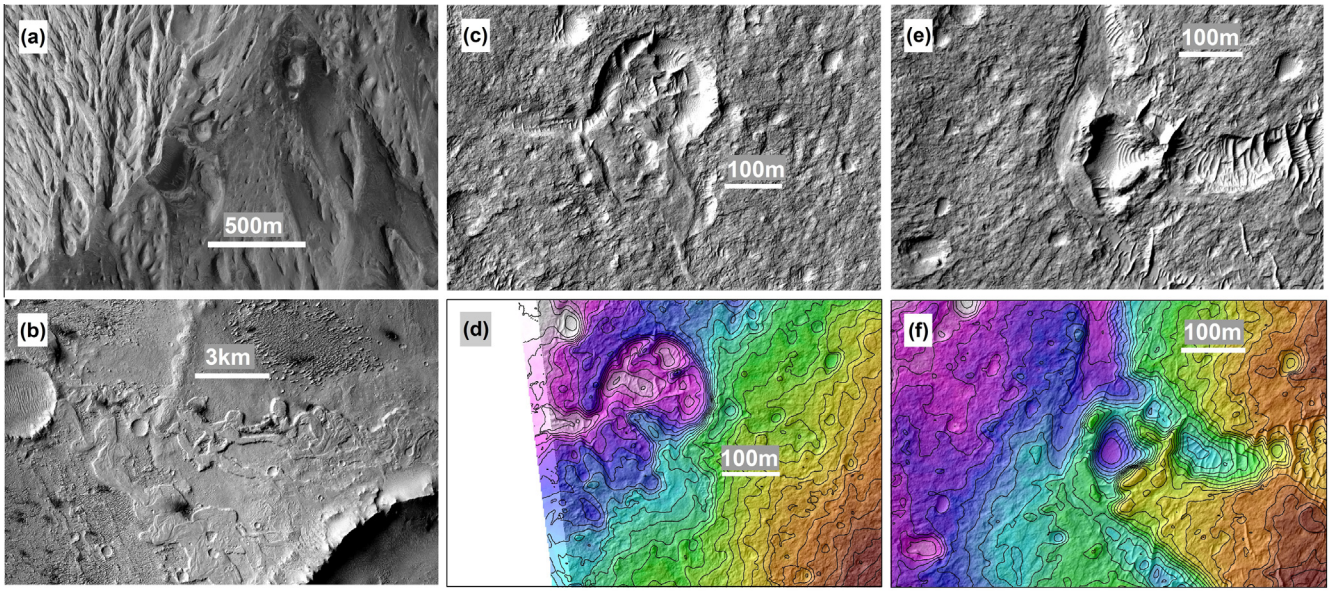

Fig. 1. Gallery of ancient martian craters. (a) Crater being exhumed from beneath an unconformity within Gale Crater's mound (Mt. Sharp, Aeolis Mons), ESP_019988_1750. (b) Craters with fresh-appearing ejecta being exhumed from beneath meander belts, Aeolis Dorsa, P15_006973_1742_XI _05S205W; Burr et al. (2010). (c) Crater being exhumed from beneath fluvial channel deposit, Aeolis Dorsa. #6 in Supplementary table, 238 m diameter. (d) Crater draped by fluvial channel deposit, Aeolis Dorsa, ESP_019104_1740. #3 in Supplementary table, 141 m diameter. (e) Crater from (c), but with 1 m elevation contours from 1 m DTM. DTM is composed of ESP_019104_1740 and ESP_017548_1740. (f) Crater from (d), with 1 m contours from the same DTM.

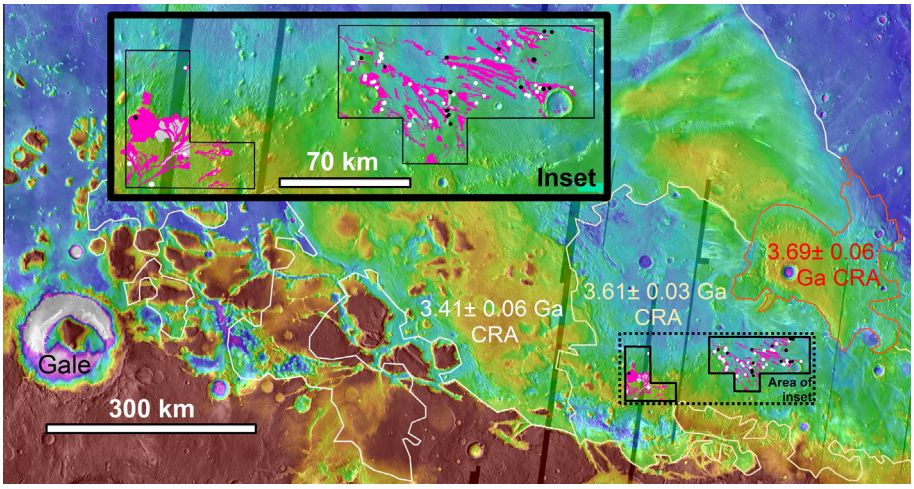

Fig. 2. Count region (black polygons outlining bright pink areas) in relation to Gale Crater and to areas with Crater-Retention Ages (CRAs) determined by Zimbelman and Scheidt (2012). Color scale corresponds to MOLA elevation, is linear, and saturates at −1000 m (red) and −3500 m (white). Orange-outlined area ("3.69±0.06 Ga CRA") is typically 500 m higher than the fluvial-channel deposits. Gale's lower mound accumulated at the same time, within error (Thomson et al., 2011). Inset shows zoom on count region. Within the count region, bright pink areas correspond to counted fluvial-channel deposits, black circles to embedded craters associated with those fluvial deposits, white circles to possible embedded craters, and gray areas to "holes" (areas not counted due to poor preservation) within fluvial-channel deposits. Circles representing craters are not to scale. Only a small subset of fluvial-channel deposits was used for this count (Burr et al., 2009). (For interpretation of the references to color in this figure legend, the reader is referred to the web version of this article.)

minimum model age of 3.69 (+0.05/−0.07) Gyr (Zimbelman and Scheidt, 2012, using the Ivanov (2001) production function and the Hartmann and Neukum, 2001 chronology function). It forms part of an eroded deposit that is thought to be Late Noachian or Early Hesperian in age (Irwin et al., 2004). These dates correlate the Aeolis rivers to the Noachian–Hesperian transition and to the lower Gale Crater mound (Fassett and Head, 2008; Kerber and Head, 2010; Thomson et al., 2011; Zimbelman and Scheidt, 2012).

The martian rivers are qualitatively similar to meandering-river deposits on Earth. Interactions with craters are, therefore, easily recognized as anomalous. Impact craters are identified by random distribution across the landscape, obliteration of older geological structures within the crater, and especially circularity and upturned rims. Interfluve material would be interpreted as overbank material (fine-grained deposits from levee-overtopping floods) if this were a basin on Earth. However, in the absence of grain-size data or diagnostic levee-breach features, wind-blown dust and silt cannot be ruled out (Haberlah et al., 2010). Locally the range in elevation spanned by deposits containing fluvial channels is >100 m. Because the dips of the river-deposit bounding surfaces are modest, the corresponding stratigraphic thickness (Δz) is similarly >100 m. Regionally, channel deposits are exposed over a ~1 km

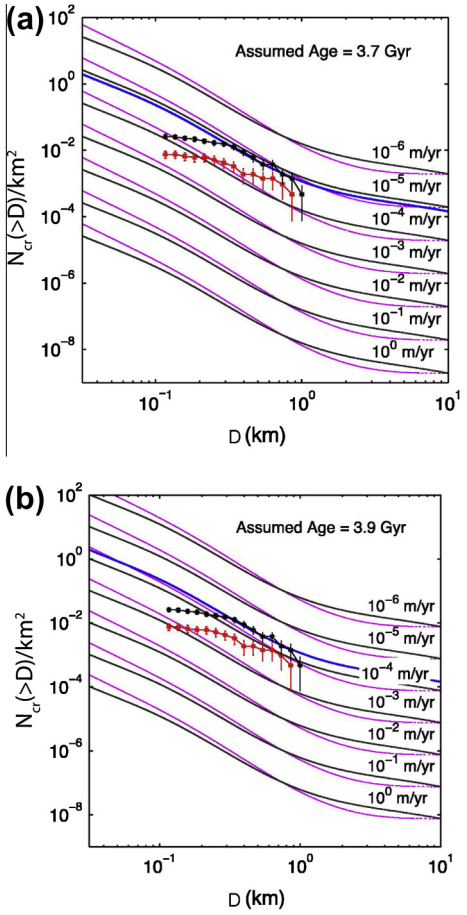

Fig. 3. Aeolis Dorsa crater–river interaction frequency: crater counts plotted against sedimentation rate curves for (a) assumed age 3.7 Gyr and (b) assumed age 3.9 Gyr. Red lines with symbols correspond to counts of definite river–crater interactions (Supplementary table); black lines with symbols correspond to counts including all candidates. Curves correspond to lines of equal sedimentation rate using crater production functions and chronology functions given by Werner and Tanaka (2011). Thin magenta lines employ Ivanov (2001) crater production function and Hartmann and Neukum (2001) chronology function. Thin black lines employ Hartmann (2005) crater production function and Hartmann (2005) chronology function (see footnote 1). 1σ-error bars assume Poisson statistics (Sivia, 2006, p. 121). Thick blue lines correspond to best-fitting accumulation rates. (For interpretation of the references to color in this figure legend, the reader is referred to the web version of this article.)

elevation range, but postdepositional modification complicates reconstruction of Δz (Lefort et al., 2012). A likely lower bound on Δz is the difference between the modern surface and a surface interpolated inward from low points surrounding the fluvial region (using a inverse-distance-weighted grid constrained to Mars Orbiter Laser Altimeter – MOLA – Precision Experimental Data Record points). This gives $\Delta z \gtrsim 300$ m.

Seventeen exhumed craters are found (Supplementary table) at multiple stratigraphic levels within 2100 km^2 of fluvial deposits surveyed with CTX images (5–6 m/pixel). Identifications were checked where possible with higher-resolution images (HiRISE or MOC). In addition to these features that are definitely identified as embedded within the stratigraphy and having definite impact crater morphology, an additional 43 candidates were found. Crater diameters were obtained by fitting a circle to the visible arc of the crater edge. The embedded-crater size–frequency distribution for $D > 250$ m (D is diameter) has a cumulative power–law slope slightly shallower than -2, $\sim$1 less than the production–function slope of -3 in this range. This is expected for a crater population embedded within a volume, as previously noted for subsurface fault populations (Yielding et al., 1996), because the fraction of embedded craters that are exposed at the $\sim$horizontal deflation surface is proportional to the absolute difference between their rim and floor elevations, which is greater for large than for smaller craters. (A pristine crater population on a geologically stable surface would parallel the production function.) Craters $D \lesssim 250$ m are still further underrepresented, which we interpret as the result of survey incompleteness, atmospheric filtering (Kite et al. 2013c), or poor.

3. Constraints on sedimentation rate and fluvial timescales

We make the following initial assumptions:

(i) Cratering is a Poisson process with an initial crater depth, $d \approx 0.2D$ for $D < 1$ km (Melosh, 1989). (HiRISE DTM measurements support this d/D for fresh Mars craters; Wes Watters, via e-mail).
(ii) Erosion does not preferentially expose craters for counting (this would increase the effective d/D).
(iii) During deflation of the deposit an embedded crater is invisible until the deflation surface reaches the embedded-crater rim. It is then visible at its original diameter until the deflation surface reaches the level of the bottom of the crater.

We discuss possible violations of these assumptions later.

The flux of impact craters at the time the deposit was forming, $f(D > D_i)$, is obtained using the crater-production and crater-chronology functions recommended by Werner and Tanaka (2011), with one exception.[1] Differences between the Hartmann and Ivanov/Neukum–Hartmann functions lead to <30% disagreement in resurfacing rate for the size-range of craters used here (Fig. 3), which is unimportant compared to other uncertainties. The expected number of embedded craters that outcrop at the modern surface, N_{cr}, is given by

$$N_{cr}(D > D_i) = f(D > D_i)(d/D)Da/S$$

where a is count area, and S is accumulation rate. Excluding $D < 290$ m craters and assuming an age in the range 3.7–3.9 Gyr, fitting of accumulation rates to the data (Fig. 3) gives $S = 50$–200 μm/yr (or 13–50 μm/yr including all candidates). Therefore, $S \approx 13$–200 μm/yr for the range of likely ages.

The most important uncertainty is f. The Aeolis Dorsa river deposits were emplaced during a period of higher crater flux f when rapid changes in f are also possible, potentially associated with the Late Heavy Bombardment. Therefore, small changes in the age of the deposit may lead to large changes in S (Werner and Tanaka, 2011). Crater-chronology functions are defined based on the lunar sample collection, whose interpretation is somewhat model-dependent, and the translation of these data to Mars is challenging (Ivanov, 2001; Robbins, 2013).

Other uncertainties tend to lead to an underestimate of exhumed-crater frequency. (a) If channel belts aggraded faster than interfluves and are erosionally resistant, and erosion is by vertical downcutting uncorrelated with laterally adjacent terrain, then at any given time the modern deflation surface will preferentially expose the erosion-resistant, crater-deficient units. In this case our procedure would underestimate the frequency of craters per unit volume averaged over the basin. On Earth, channel belts always aggrade faster than their floodplains on interannual timescales, but levee breaches and avulsions maintain constant aggradation rate

[1] The chronology function given for Hartmann (2005) by Werner and Tanaka (2011) is in error. Instead, we use $N(1) = 3.79 \times 10^{-14}(\exp(6.93t) - 1) + 5.84 \times 10^{-4}t$ (here, t is in Gyr).

across the floodplain averaged over depths greater than ~1 channel depth (Mohrig et al., 2000). Channel-width measurements (Burr et al., 2010), standard fluvial scaling relations, and our HiRISE DTM measurements of negative-relief channel depths all indicate that Aeolis channel depths should be small compared to the original depth of the craters in our count (i.e. channel depth ≪30–60 m). Therefore lateral gradients in sedimentation rate are unlikely to be important if the interfluves are floodplain deposits. (b) Cliff-forming units that are very resistant to vertical abrasion will be removed by lateral mass wasting as surrounding weaker material is eroded. In this case, no embedded craters within those cliff-forming units will be included in the count: craters on top of the cliff-forming units will be hard to distinguish from relatively recent synerosional craters, and craters within those units will be blanketed by talus throughout the erosion process. Only craters on the substrate that have been partially exhumed from beneath the cliff-forming unit will be visible, and so the effective count area then scales with the perimeter of the cliff-forming unit, rather than with its area. (c) S would halve in the extreme case that all craters initially have a secondary-like d/D (i.e., ~0.1). d/D is currently <0.1 in our HiRISE DTMs, but this could be due to incomplete erosion or recent infilling. (d) Supposing small craters were all erosionally resistant and formed mesas as tall as their diameter, assumption (iii) would be violated and a surface count would overestimate the true crater density. However, our CTX and HiRISE DTMs show that small exhumed craters are not locally highstanding in this region, although they do tend to be preserved with rims intact, so (iii) is probably a good approximation. (e) We assume craters are either present at full diameter or eliminated completely, but the apparent diameter of an eroding crater may be less (or more) than its initial diameter. (f) Finally, we neglect possible erosion of craters *during* the period of net accumulation.

Because these errors tend to lead to an underestimate of the number and size of craters that formed during the interval of fluvial deposition, we interpret our data as a lower limit on time for accumulation. Assuming $\Delta z \gtrsim 300$ m, the range of minimum deposition timescale is $\Delta z/S \sim 1$–20 Myr for the range of likely ages (or 0.6–40 Myr assuming a wider range of age uncertainty, from 3.6 to 4.0 Gyr).[2]

4. Discussion

The simplest interpretation of these data is fluvial aggradation at rates comparable to Earth (fluvial aggradation rates ranging from 50 to 600 μm/yr are compiled from Earth data by Miall (2012)). Aeolis Dorsa sedimentation cannot be distinguished from later sedimentation on the basis of sedimentation rate alone. Putzig et al. (2009) correlate radar reflectors within the North Polar Layered Deposits to obliquity cycles over the last 4 Ma and obtain $S \sim 1$ mm water ice/yr. Similarly, Lewis et al. (2008) correlate bed:bundle ratios in Becquerel Crater at 22°N to Milankovitch beats and obtain $S \sim 30$ μm/yr. Typical equatorial mound rhythmic-layer thicknesses of 3–20 m (Lewis et al., 2010) imply accumulation at 20–200 μm/yr if forced by obliquity cycles (0.12 Myr), or 100–800 μm/yr if forced by precession (0.025 Myr effective period at the equator). Zabrusky et al. (2012) find $S > 3$ μm/yr in Meridiani using pedestal craters. Rhythmites have been hypothesized to be relatively young (Grotzinger and Milliken, 2012). Modern gross sedimentation rate on Mars is 10–100 μm/yr from dust storms (e.g., Drube et al., 2010).

On Earth, mean sedimentation rate frequently decreases with increasing measurement duration (Jerolmack and Sadler, 2007) as a result of power–law fluctuations of the boundary between erosion and deposition (Schumer and Jerolmack, 2009). This "Sadler effect" is ubiquitous at short timescales near coasts but is less relevant on the longest timescales, or where erosion is unimportant (Jerolmack and Sadler, 2007). It is not clear whether the Sadler effect should apply to Mars sediments. Martian weather is remarkably predictable on both synoptic and interannual timescales, probably because of the lack of a large energy capacitor analogous to Earth's ocean (Read and Lewis, 2004). Therefore, we might speculate that Mars' sedimentary record, as the imprint of the atmosphere on rocks, is less chaotic than its Earth counterpart. Consistent with this, quasi-periodic bedding is common on Mars (Lewis et al., 2010) and angular unconformities are rare. CTX images suggest that exhumed craters in this region are concentrated at a few stratigraphic levels, consistent with omission surfaces.

The sediment source for the Aeolis Dorsa deposits is uncertain, and so it is not clear whether the accumulation of the deposits was rate-limited by fluvial transport or by aeolian transport. One option is that sediment was fluvially transported from highlands to the south. The volume of valley networks draining toward Aeolis Dorsa appears to be much smaller than the volume of the clastic wedge, and no complete transport pathways are visible (however, the volume of valley networks is only a lower bound on the total fluvially-eroded volume). It is conceivable that the Aeolis Dorsa deposits are fluvially reworked ancient highlands crust, which would require that the dichotomy boundary was once further to the north. But crater-floor tilts suggest that the dichotomy boundary was in place near its current location prior to the late Noachian (Watters et al., 2007). An attractive possibility is that the fluvial deposits are reworked from relatively weak aeolian or niveoaeolian deposits accumulating at the highland–lowland boundary (Irwin et al., 2004).

The relatively low embedded-crater frequency demonstrates that sedimentary processes on Mars could outcompete cratering even when the impact flux was higher early in Solar System history (Howard, 2007). This is in line with low Platinum Group Element concentrations in 3.8 Ga metasediments from Earth (Anbar et al., 2001).

5. Implications for ancient climate and MSL's mission to Gale Crater

A lower bound of 1–20 Myr for the total interval spanned by fluvial deposition rules out basin-filling by a single catastrophic episode, and is consistent with hydrologic and total-erosion estimates for fluvial activity around the Noachian–Hesperian boundary (e.g., Barnhart et al., 2009; Hoke et al., 2011). Possible climate regimes include multiple climate transients (Segura et al., 2008; Wordsworth et al., 2013), or intermittent precipitation-fed runoff over $\geqslant 10^5$ yr (Barnhart et al., 2009). The sedimentary rock record of Mars appears to record a small fraction of Mars history, perhaps because surface liquid water was necessary for lithification and was only available intermittently (Moore, 1990; Knoll et al., 2008; Andrews-Hanna and Lewis, 2011; Kite et al., 2013a).

Based on observed and candidate embedded-crater frequency in Aeolis Dorsa, we predict an Aeolis Mons (Mount Sharp) sedimentation rate of $\lesssim$13–200 μm/yr, including nondepositional intervals, averaged over the ~2 km-thick lower mound. This assumes that sedimentation rates across the broader Aeolis region were fairly uniform. Our prediction is testable with MSL measurements of cosmogenic noble gases (e.g., Shuster et al., 2012), meteoritic Ni (Yen et al., 2006), meteoritic organic matter (OM), and

[2] Our constraint is slightly tighter than that given in our preprint arXiv:1207.6726v1, because we have used an improved fitting procedure, used denser grids for interpolation, and corrected an error in the Werner and Tanaka (2011) chronology functions.

small embedded craters. Mars Hand Lens Imager's (MAHLI's) 14 μm-per-pixel resolution permits identification of $\geqslant$40 μm-thick varves, if they exist.

River deposits exist at the Gale mound, but those clearly identifiable from orbit appear to postdate the accumulation of the lower unit of Aeolis Mons. It has been argued that the primary sediment source for the Gale mound is atmospherically-transported sediment (Pelkey et al., 2004; Thomson et al., 2011; Kite et al., 2013b). If this is true, then the extrapolation of the Aeolis Dorsa sedimentation rate to Aeolis Mons depends on the assumption that river sedimentation in the Aeolis Dorsa region was supply-limited, with sediment introduced to the region by aeolian processes (e.g., Irwin et al., 2004; Haberlah et al., 2010).

Sediment accumulation rate affects the hunt for OM on Mars. Fast sedimentation dilutes OM delivered by meteoritic infall – thus reducing the "meteoritic background level" (Summons et al., 2011). Preservation of OM introduced at the surface is affected by time-to-burial to a depth of order 1 m. During this time, OM is vulnerable to degradation by radiation, atmospheric oxidants, and/or UV, to an extent that depends on the unknown redox state, composition and thickness of early Mars' atmosphere (Pavlov et al., 2012). On Earth, overbank environments and oxbow lakes in meander belts are favored among subaerial environments for preserving organic matter (Summons et al., 2011).

Future work might use MSL data and further orbital analyses to assess the relation between exposure time, crater frequency, OM preservation, and atmospheric paleopressure. The existence of >3.7 Gyr-old, $\leqslant 10^2$ m-diameter craters should place an upper limit on ancient atmospheric pressure, because small impactors do not form hypervelocity craters beneath thick atmospheres (Popova et al., 2003); we are pursuing this quantitatively (Kite et al., 2013c).

Acknowledgments

We thank Mike Lamb, Ken Farley, the participants in Caltech's Mars Fluvial Geomorphology Reading Group, Devon Burr, Alexandra Lefort, Robert Jacobsen, Wes Watters, and especially Oded Aharonson, Mark Allen, Woody Fischer, Kevin Lewis, and Nick Warner, for discussions. We additionally thank Kevin Lewis and Oded Aharonson for sharing their preprint on cyclic bedding. We thank two anonymous reviewers for their comments, and Jeff Moersch for editorial handling. We thank the HiRISE team for maintaining a responsive public target request program, HiWish, which was useful for this work. DTMs produced for this work, ESP_17548_1740/ESP_019104_1740 (@1 m/pixel) and PSP_007474_1745/ESP_024497_1745 (@2.5 m/pixel) are available for unrestricted further use from the corresponding author.

Appendix A. Supplementary material

Supplementary data associated with this article can be found, in the online version, at http://dx.doi.org/10.1016/j.icarus.2013.03.029.

References

Anbar, A.D. et al., 2001. Extraterrestrial iridium, sediment accumulation and the habitability of the early Earth's surface. J. Geophys. Res. 106, 3219–3236.
Andrews-Hanna, J.C., Lewis, K.W., 2011. Early Mars hydrology: 2. Hydrological evolution in the Noachian and Hesperian epochs. J. Geophys. Res. 116, E02007.
Barnhart, C.J. et al., 2009. Long-term precipitation and late-stage valley network formation: Landform simulations of Parana Basin, Mars. J. Geophys. Res. 114, E01003.
Burr, D.M. et al., 2009. Pervasive aqueous paleoflow features in the Aeolis/Zephyria Plana region, Mars. Icarus 200, 52–76.
Burr, D.M. et al., 2010. Inverted fluvial features in the Aeolis/Zephyria Plana region, Mars: Formation mechanism and initial paleodischarge estimates. J. Geophys. Res. 115, E07011.
Drube, L. et al., 2010. Magnetic and optical properties of airborne dust and settling rates of dust at the Phoenix landing site. J. Geophys. Res. 115, E00E23.
Edgett, K.S., 2005. The sedimentary rocks of Sinus Meridiani. Mars J. 1, 5–58.
Edgett, K. S., & Malin, M. C., 2002. Martian sedimentary rock stratigraphy, Geophys. Res. Lett., 29, 32-1–32-4.
Fassett, C.I., Head, J.W., 2008. The timing of martian valley network activity: Constraints from buffered crater counting. Icarus 195, 61–89.
Fassett, C.I., Head, J.W., 2011. Sequence and timing of conditions on early Mars. Icarus 211, 1204–1214.
Grant, J.A., Wilson, S.A., 2011. Late alluvial fan formation in southern Margaritifer Terra, Mars. Geophys. Res. Lett. 38, L08201.
Grotzinger, J.P., Milliken, R.E., 2012. The sedimentary rock record of Mars. In: Grotzinger, J.P., Milliken, R.E. (Eds.), Sedimentary Geology of Mars. SEPM Special Publication No. 102, pp. 1–48.
Haberlah, D. et al., 2010. Loess and floods: High-resolution multi-proxy data of Last Glacial Maximum (LGM) slackwater deposition in the Flinders Ranges, semi-arid South Australia. Quatern. Sci. Rev. 29, 2673–2693.
Hartmann, W.K., 2005. Martian cratering 8: Isochron refinement and the chronology of Mars. Icarus 175, 294–320.
Hartmann, W.K., Neukum, G., 2001. Cratering chronology and the evolution of Mars. Space Sci. Rev. 96, 165–194.
Hoke, M.R.T. et al., 2011. Formation timescales of large martian valley networks. Earth Planet. Sci. Lett. 312, 1–12.
Howard, A., 2007. Simulating the development of martian highland landscapes through the interaction of impact cratering, fluvial erosion, and variable hydrologic forcing. Geomorphology 91, 332–363.
Irwin, R.P. et al., 2004. Sedimentary resurfacing and fretted terrain development along the crustal dichotomy boundary, Aeolis Mensae, Mars. J. Geophys. Res. 109, E09011.
Irwin III, R.P. et al., 2005. An intense terminal epoch of widespread fluvial activity on early Mars: 2. Increased runoff and paleolake development. J. Geophys. Res. 110, E12S15.
Ivanov, B.A., 2001. Mars/Moon cratering rate ratio estimates. Space Sci. Rev. 96, 87–104.
Jerolmack, D.J., Sadler, P., 2007. Transience and persistence in the depositional record of continental margins. J. Geophys. Res. 112, F03S13.
Kerber, L., Head, J.W., 2010. The age of the Medusae Fossae Formation. Icarus 206, 669–684.
Kite, E.S. et al., 2011. Localized precipitation and runoff on Mars. J. Geophys. Res. 116, E07002.
Kite, E.S. et al., 2013a. Seasonal melting and the formation of sedimentary rocks on Mars, with predictions for the Gale Crater mound. Icarus 223, 181–210.
Kite, E.S. et al., 2013b. Growth and form of the mound in Gale Crater, Mars: Slope-wind enhanced erosion and transport. Geology. http://dx.doi.org/10.1130/G33909.1.
Kite, E.S., Williams, J.-P., Lucas, A., & O. Aharonson, 2013c. Constraints on early Mars atmospheric pressure from small ancient craters, arXiv, astro-ph:EP, http://arxiv.org/abs/1304.4043.
Knoll, A.H. et al., 2008. Veneers, rinds, and fracture fills: Relatively late alteration of sedimentary rocks at Meridiani Planum, Mars. J. Geophys. Res. 113 (E6), E06S16.
Lefort, A., Burr, D.M., Beyer, R.A.,Howard, A.D., 2012. Inverted fluvial features in the Aeolis–Zephyria Plana, Western Medusae Fossae Formation, Mars: Evidence for post-formation modification. J. Geophys. Res. 117, p. 24. http://dx.doi.org/10.1029/2011JE004008.
Lewis, K.W. et al., 2008. Quasi-periodic bedding in the sedimentary rock record of Mars. Science 322, 1532–1535.
Lewis, K.W. et al., 2010. Global Significance of Cyclic Sedimentary Deposits on Mar. Lunar Planet Sci. 41. Abstract #2648.
Mangold, N. et al., 2012. The origin and timing of fluvial activity at Eberswalde crater, Mars. Icarus 220, 231–251.
Matsubara, Y. et al., 2011. Hydrology of early Mars: Lake basins. J. Geophys. Res. 116, E04001.
Melosh, H.J., 1989. Impact Cratering: A Geologic Process. Oxford University Press, New York.
Miall, A.D., in press. Updating uniformitarianism: Stratigraphy as just a set of "Frozen accidents", in Smith, D. G., Bailey, R., J., Burgess, P., and Fraser, A., eds., Strata and time: Geological Society, London Special Publication.
Mohrig, D. et al., 2000. Interpreting avulsion process from ancient alluvial sequences: Guadalope–Matarranya system (northern Spain) and Wasatch formation (western Colorado). Geol. Soc. Am. Bull. 112, 1787–1803.
Moore, J.M., 1990. Nature of the mantling deposit in the heavily cratered terrain of northeastern Arabia, Mars. J. Geophys. Res. 95, 14279–14289.
Pavlov, A.A., et al. Degradation of the organic molecules in the shallow subsurface of Mars due to irradiation by cosmic rays, Geophys. Res. Lett. 39, L13202, http://dx.doi.org/10.1029/2012GL052166.
Pelkey, S.M. et al., 2004. Surficial properties in Gale Crater, Mars, from Mars Odyssey THEMIS data. Icarus 167, 244–270.
Popova, O. et al., 2003. Bolides in the present and past martian atmosphere and effects on cratering processes. Meteor. Planet. Sci. 38, 905–925.
Putzig, N. et al., 2009. Subsurface structure of Planum Boreum from Mars Reconnaissance Orbiter Shallow Radar soundings. Icarus 204, 443–457.
Read, P.L., Lewis, S.R., 2004. The Martian Climate Revisited: Atmosphere and Environment of a Desert Planet. Springer-Praxis.
Robbins, S.J., 2013. Revised lunar cratering chronology for planetary geological histories. Lunar Planet Sci. 44. Abstract 1619.

Sagan, C., Mullen, G., 1972. Earth and Mars: Evolution of atmospheres and surface temperatures. Science 177, 52–56.
Schumer, R., Jerolmack, J.D., 2009. Real and apparent changes in sediment deposition rates through time. J. Geophys. Res. 114, F00A06.
Segura, T.L. et al., 2008. Modeling the environmental effects of moderate-sized impacts on Mars. J. Geophys. Res. 113, E11007.
Segura, T.L. et al., 2012. An impact-induced, stable, runaway climate on Mars. Icarus 220, 144–148.
Shuster, D.L. et al., 2012. Cosmogenic ^{3}He in hematite and goethite from Brazilian "canga" duricrust demonstrates the extreme stability of these surfaces. Earth Planet. Sci. Lett. 329, 41–50.
Sivia, D.S., 2006. Data Analysis: A Bayesian Tutorial, second ed. Oxford University Press.
Smith, M.R. et al., 2008. Effect of obliteration on crater-count chronologies for martian surfaces. Geophys. Res. Lett. 35, L10202.
Summons, R.E. et al., 2011. Preservation of martian organic and environmental records. Astrobiology 11, 157–181.
Thomson, B.J. et al., 2011. Constraints on the origin and evolution of the layered mound in Gale Crater, Mars using Mars Reconnaissance Orbiter data. Icarus 214, 413–432.
Toon, O.B., Segura, T., Zahnle, K., 2010. The formation of martian river valleys by impacts. Ann. Rev. Earth Planet. Sci. 38, 303–322.
Watters, T.R. et al., 2007. Hemispheres apart: The crustal dichotomy on Mars. Ann. Rev. Earth Planet. Sci. 35, 621–652.
Werner, S.C., Tanaka, K.L., 2011. Redefinition of the crater-density and absolute-age boundaries for the chronostratigraphic system of Mars. Icarus 215, 603–607.
Wordsworth, R. et al., 2013. Global modelling of the early martian climate under a denser CO_2 atmosphere: Water cycle and ice evolution. Icarus 222, 1–19.
Yen, A.S. et al., 2006. Nickel on Mars: Constraints on meteoritic material at the surface. J. Geophys. Res. 111, E12S11.
Yielding, G. et al., 1996. Sampling of fault populations using sub-surface data: A review. J. Struct. Geol. 18, 135–146.
Zabrusky, K., Andrews-Hanna, J.C., Wiseman, S., 2012. Reconstructing the distribution and depositional history of the sedimentary deposits of Arabia Terra, Mars. Icarus 220, 311–330.
Zimbelman, J.R., Scheidt, S.P., 2012. Hesperian age for Western Medusae Fossae Formation, Mars. Science 336, 1683.